Published online 23 September 2023

NAR Cancer, 2023, Vol. 5, No. 3 **1**
https://doi.org/10.1093/narcan/zcad049

Specificity of cancer-related chromosomal translocations is linked to proximity after the DNA double-strand break and subsequent selection

Reynand Jay Canoy[1,2,†], Anna Shmakova[1,3,4,†], Anna Karpukhina[1,4], Nikolai Lomov[5], Eugenia Tiukacheva[1,4], Yana Kozhevnikova[1], Franck André[1], Diego Germini[1,*] and Yegor Vassetzky[1,4,*]

[1]UMR 9018, CNRS, Univ. Paris-Sud, Université Paris Saclay, Institut Gustave Roussy, F-94805 Villejuif, France, [2]Institute of Human Genetics, National Institutes of Health, University of the Philippines Manila, 1000 Manila, The Philippines, [3]Laboratory of Molecular Endocrinology, Institute of Experimental Cardiology, Federal State Budgetary Organization 'National Cardiology Research Center' of the Ministry of Health of the Russian Federation, 127994 Moscow, Russia, [4]Koltzov Institute of Developmental Biology, 117334 Moscow, Russia and [5]Department of Molecular Biology, Faculty of Biology, Lomonosov Moscow State University, 119991 Moscow, Russia

Received March 17, 2023; Revised August 01, 2023; Editorial Decision August 30, 2023; Accepted September 14, 2023

ABSTRACT

Most cancer-related chromosomal translocations appear to be cell type specific. It is currently unknown why different chromosomal translocations occur in different cells. This can be due to either the occurrence of particular translocations in specific cell types or adaptive survival advantage conferred by translocations only in specific cells. We experimentally addressed this question by double-strand break (DSB) induction at *MYC*, *IGH*, *AML* and *ETO* loci in the same cell to generate chromosomal translocations in different cell lineages. Our results show that any translocation can potentially arise in any cell type. We have analyzed different factors that could affect the frequency of the translocations, and only the spatial proximity between gene loci after the DSB induction correlated with the resulting translocation frequency, supporting the 'breakage-first' model. Furthermore, upon long-term culture of cells with the generated chromosomal translocations, only oncogenic *MYC–IGH* and *AML–ETO* translocations persisted over a 60-day period. Overall, the results suggest that chromosomal translocation can be generated after DSB induction in any type of cell, but whether the cell with the translocation would persist in a cell population depends on the cell type-specific selective survival advantage that the chromosomal translocation confers to the cell.

GRAPHICAL ABSTRACT

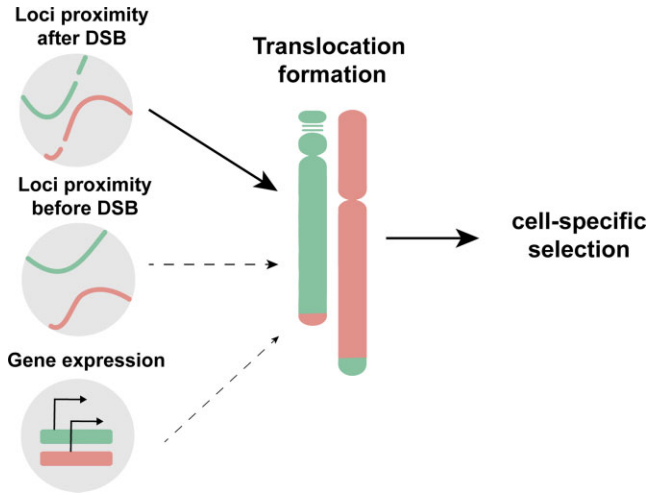

INTRODUCTION

Chromosomal translocations are hallmarks of many cancers (1). More than 50% of leukemias and almost all lymphomas exhibit or are directly caused by chromosomal translocations (2–5). Functional consequences of chromosomal translocations include aberrant expression of otherwise normal genes, expression of fusion genes and/or large-scale changes in the nuclear organization (6–9).

Many of the known chromosomal translocations appear to be cell type specific (3). For example, the *MYC–IGH* translocation has only been observed in B cells and not in

*To whom correspondence should be addressed. Tel: +33 1 42 11 45 26; Email: germinidiego@gmail.com
Correspondence may also be addressed to Yegor Vassetzky. Tel: +33 1 42 11 62 83; Fax: +33 1 42 11 54 94; Email: yegor.vassetzky@cnrs.fr
†The authors wish it to be known that, in their opinion, the first two authors should be regarded as Joint First Authors.

other cell types. Why do different chromosomal translocations occur in different cells? Is this due to the fact that some translocations are more likely to occur in specific cell types due to cell-specific characteristics or do translocations occur in a similar manner in all cells, but they confer a selective advantage in a specific cell type? The generation of chromosomal translocation involves two major steps: the formation of specific double-strand breaks (DSBs) and their erroneous repair via nonhomologous end joining (NHEJ) (10). Cell-specific traits that may potentially affect translocation formation include preferential occurrence of DSBs at specific loci in specific cell types [e.g. due to chromatin state or the activity of intrinsic DNA-cutting enzymes (9,11)] and/or predetermined factors that affect DNA repair [e.g. transcriptional activity, loci spatial proximity, the activity of specific repair factors or even cell-specific expression of chromosomal aberrations stimulating long noncoding RNAs (lncRNAs) (12)]. While previous studies have extensively explored the occurrence of cell-specific DSBs, less is known about the risk factors that interfere with translocation-prone DSB repair once they are already formed in a particular cell type. Chromatin state, DSB movement and DNA damage sensing and repair mechanisms influence the generation of chromosomal translocations at this step (9). The presence of specific transcripts [e.g. lncRNAs that share homology regions for two different loci (12,13)] or certain drugs (14) can also affect the formation of chromosomal rearrangements. Understanding these risk factors is crucial for developing targeted interventions to prevent the occurrence of translocations and the development of related diseases such as cancer.

Studying randomly induced and/or naturally occurring chromosomal translocations poses challenges and serious limitations. First, translocations are rare events, for certain types of translocations literally a single event occurs in the whole organism, and cells with translocations can survive and proliferate only if translocation provides a proliferative advantage in a cell population. Second, the localization of breakpoints in naturally occurring translocations varies from kilobases to hundreds of kilobases, which requires sophisticated techniques to detect them [e.g. long-range polymerase chain reaction (PCR), fluorescence *in situ* hybridization (FISH), deep sequencing, etc.] (15,16). With the advancement of gene-editing tools that can produce DSBs at specific loci, the generation of cell lines with specific chromosomal translocations became possible (14,17–22). The CRISPR/Cas9 tool generates DSBs in both euchromatin and heterochromatin regions (23–27), which facilitates the study of factors that affect the formation of translocations across different cell types. Here, we devised a CRISPR/Cas9-based experimental strategy to induce DSBs in one cell within several specific loci that are commonly involved in oncogenic chromosomal rearrangements (*MYC*, *IGH*, *AML*, *ETO*) with the aim to stimulate the formation of chromosomal translocations between these loci. Using this strategy, we investigated different factors associated with the frequency of generated chromosomal translocations in human cells of different developmental origins. We analyzed the translocation frequencies with respect to the transcription activity, nuclear radial position and spatial proximity of the gene loci targeted by CRISPR/Cas9 and demonstrated that in all of the considered cell types the most prominent factor affecting the chromosomal translocations was the spatial proximity between the potential partner loci after the DSB induction. The colocalization of potential partner loci after the DSB induction was dependent on DNA-dependent protein kinase (DNA-Pk) activity. Our results demonstrated that virtually any type of chromosomal translocation can arise in any cell type after the induction of DSBs, but the persistence of cells with these translocations is dependent on the specific survival advantage conferred by the translocation in that cell type. This highlights the complexity of chromosomal translocations in cancer cells and underscores the importance of considering the selective survival advantage of chromosomal translocations in different cell types, adding a new dimension to our understanding of the process.

MATERIALS AND METHODS

Cell culture

All cells were handled in aseptic techniques and were kept in a humidified incubator at 37°C with 5% CO_2 until use. They were maintained in their respective cell culture growth medium and were passed at least once a week. For the recipes of the growth medium, see Supplementary Data. Cell treatments are listed in Supplementary Table S1.

gRNA design, cloning and testing

All guide RNA (gRNA) binding sites were generated from CRISPOR gRNA design online tool (http://crispor.tefor.net/) (28) and were inserted into the phU6 gRNA plasmids (Addgene #53188). gRNA and Cas9 plasmids (Addgene #57818) were transformed into DH5α competent cells via heat shock and were then subsequently clonally expanded for plasmid extraction (Machery-Nagel NucleoBond Xtra Midi or Maxi kit). gRNA efficiency was tested following the procedures provided in TIDE (29) and ENIT (30) protocols. For the sequences of the gRNA binding sites, see Supplementary Table S2.

Electrotransfection

Cells were electrotransfected following the protocol for hard-to-transfect cells in (31). Briefly, 4–8 × 10^6 cells were electrotransfected with 50 μg total plasmid, 60% of which is Cas9 and the remaining 40% consists of gRNA plasmids. After 2 days, electrotransfection efficiency was checked using Accuri™ C6 Flow Cytometer (BD Biosciences). Depending on the intended number of electrotransfected cells, the electrotransfection reactions were scaled up.

Western blot

Western blot analysis was performed following the protocol in (32) using the following antibodies: Cas9 antibody (7A9-3A3) (anti-mouse, Santa Cruz Biotechnology, sc-517386), GAPDH (anti-mouse, Cell Signaling Technology, 2118) and anti-mouse peroxidase-conjugated secondary antibodies (Jackson ImmunoResearch, 315035003).

PCR and qPCR

Total DNA was extracted using NucleoSpin Tissue DNA purification kit (Macherey-Nagel) following the manufacturer's protocol. Total RNA was extracted using NucleoSpin RNA II purification kit (Macherey-Nagel) and was then converted to complementary DNA (cDNA) using Maxima H Minus cDNA Synthesis Master Mix (Thermo Fisher Scientific) following the manufacturer's protocol. PCR amplification was performed using PowerUp SYBR Green Master Mix (Thermo Scientific) following the manufacturer's protocol. For the PCR primers used, see Supplementary Tables S3 and S4.

Translocation frequency was calculated using the Pfaffl method (33) to correct for the observed varying amplification efficiencies of each primer pair (Supplementary Figure S2F). The calculated frequencies were then adjusted to the respective transfection efficiencies measured 2 days after electrotransfection, right before cell collection, using the Accuri™ C6 Flow Cytometer (BD Biosciences).

3D-FISH

3D-FISH was performed following the protocols in (18) using the following probes: AML (Empire Genomics, RP11-1056O16 blue), ETO (Empire Genomics, RP11-643O11 orange), MYC (Empire Genomics, RP11-440N18 red) and IGH (Empire Genomics, RP11-346I20 green). For image acquisition and analysis, see Supplementary Data.

Statistical analysis

All experiments were performed with at least two biological replicates and two technical replicates. Statistical analyses were performed using GraphPad Prism 9.1.0.221 and R Studio. For comparisons between the two groups, an unpaired *t*-test was done. For comparisons involving more than two groups, one-way analysis of variance (ANOVA) and Tukey's honest significant difference as the post-hoc test were performed. For the correlation analysis, the Spearman correlation between the translocation frequency and the predictors (gene expression/loci proximity before DSB/loci proximity after DSB) was performed.

RESULTS

Experimental strategy for analysis of CRISPR/Cas9-induced chromosomal translocations

With the aim to identify factors affecting the generation of chromosomal translocations across cell types, we developed a CRISPR/Cas9-based strategy to induce DSBs in one cell within several chromosomes. This would potentially generate several different chromosomal translocations upon erroneous repair of these DSBs via NHEJ (Figure 1A and Supplementary Figure S1A). The frequencies of induced chromosomal translocations were measured by quantitative PCR (qPCR) and compared in one cell type and between different cell types. We selected four loci for DSB induction: the *RUNX1T1* (formerly known as *ETO*) gene on chromosome 8q21, the upstream region of the *MYC* gene on chromosome 8q24, the immunoglobulin heavy chain (*IGH*) gene locus on chromosome 14q32 and the *RUNX1* (formerly known as *AML*) gene on chromosome 21q22. These gene loci are involved in clinically relevant oncogenic translocations: t(8;21) between *AML* and *ETO* in acute myeloid leukemia and t(8;14) between *MYC* and *IGH* in Burkitt's lymphoma.

The gRNAs were designed (Supplementary Table S2) to target the above loci and cloned into phU6 plasmids. gRNA efficiency was tested by TIDE (29) as described in the 'Materials and Methods' section and gRNAs with similar efficiencies were chosen to avoid a bias of different CRISPR/Cas9 cutting efficiencies (Supplementary Figure S2A). The cells were then electrotransfected with the Cas9-expressing plasmid to determine the Cas9 expression kinetics. The Cas9 expression started to peak 48 h after the electrotransfection (Supplementary Figure S2B). We then tested the cell survival and apoptosis after electrotransfection (Supplementary Figure S2C and D).

We designed PCR primers (Supplementary Tables S3 and S4) to detect resulting translocations. Supplementary Figure S2E shows a representative image of an agarose gel electrophoresis of PCR-amplified *MYC–IGH* translocations after electrotransfection with Cas9 and gRNAs targeting the *MYC* and *IGH*, *AML–ETO* translocations after electrotransfection with Cas9 and gRNAs targeting the *AML* and *ETO*, *IGH–ETO* translocations after electrotransfection with Cas9 and gRNAs targeting the *IGH* and *ETO*, and *AML–IGH* translocations after electrotransfection with Cas9 and gRNAs targeting the *AML* and *IGH*. The amplification efficiencies of each primer pair (Supplementary Figure S2F) were taken into account when calculating the translocation frequency (see the 'Materials and Methods' section). The translocation frequency started peaking 48 h post-transfection (Supplementary Figure S3); therefore, we selected the 48 h post-electrotransfection as the collection time point for the next experiments to avoid the effect of positive or negative selection of translocations upon subsequent cell divisions.

We used inhibitors of specific repair pathways to determine the pathway of the translocation formation in our model. We added the inhibitors of either MRE11 involved in both classical and alternative NHEJ (mirin) or DNA-Pk involved in the canonical NHEJ pathway (NU7026). We observed that treatment with NU7026 led to a 2.4-fold increase ($P = 0.0056$) in the translocation rate (Figure 1B), suggesting that translocations are mainly due to the alternative NHEJ repair as already proposed by others (34).

Simultaneous induction of DSBs results in cell type-specific translocation frequencies

To analyze the appearance of chromosomal translocations in different cell types, we induced DSBs in cell lines of different developmental origin and ploidy: RPMI8866 (lymphoid, B cell, diploid with three to four copies of chromosome 8), Jurkat (lymphoid, T cell, diploid), K562 [myeloid, nearly triploid (35)], MRC5 (lung fibroblast, diploid) and Hek-293 (embryonic kidney, epithelial, hypotriploid). These cell lines were electrotransfected with plasmids encoding for Cas9 and gRNA combinations targeting two sets of gene loci: *MYC*, *IGH* and *AML* (MIA) or

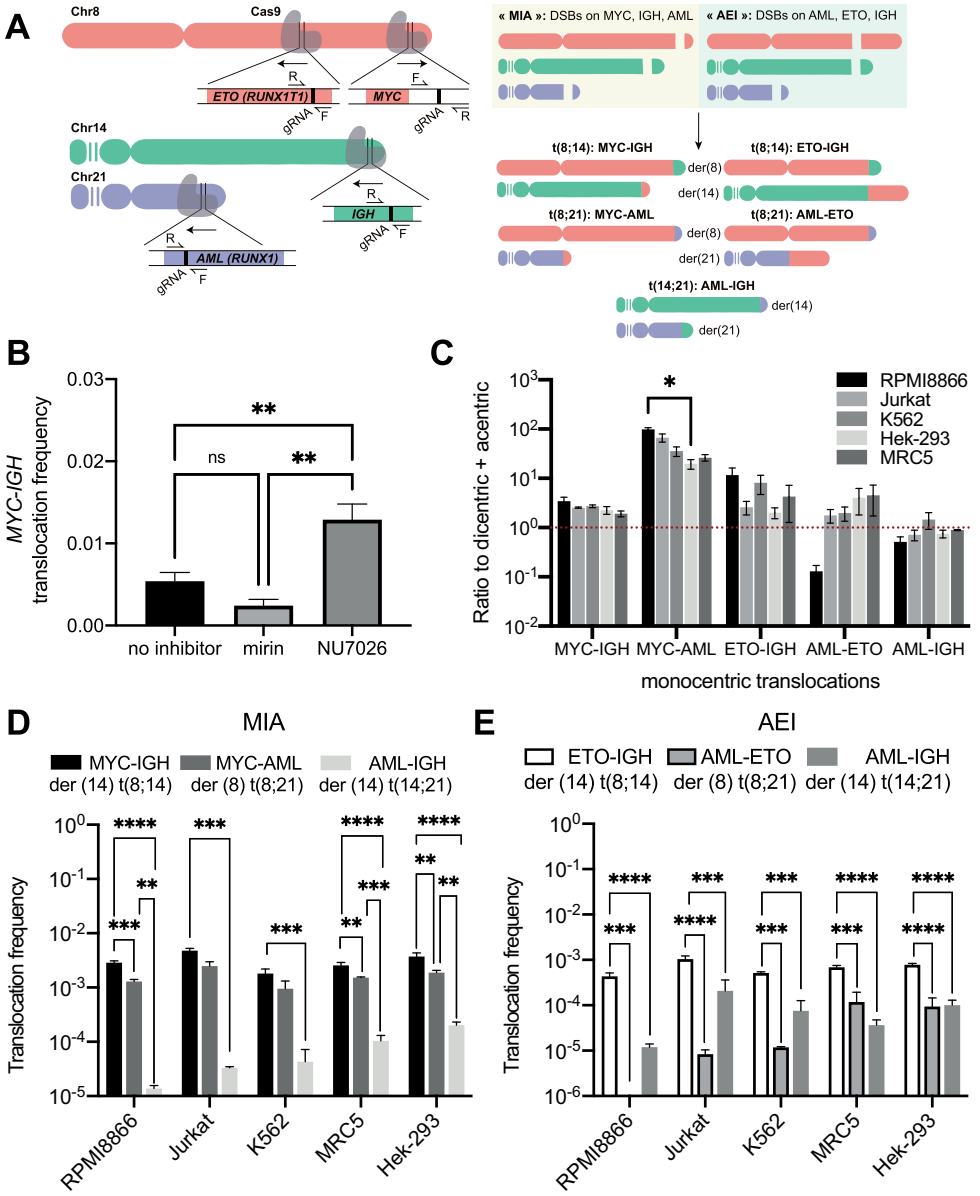

Figure 1. Translocations generated in different cells after the simultaneous induction of three DSBs on chromosomes 8, 14 and 21. (**A**) Positions of sites targeted by gRNA in the *ETO* (8q21.3), *MYC* (8q24.12), *IGH* (14q32.33) and *AML* (21q22.12) gene loci (left panel) and the resulting potential unicentric chromosomal translocations after targeting *MYC*, *IGH* and *AML* loci (MIA) or *AML*, *ETO* and *IGH* loci (AEI) (right panel). (**B**) *MYC*–*IGH* translocation frequency after inhibition of NHEJ repair components. Six hours after electrotransfection with gRNA and Cas9 plasmids, cells were treated with either mirin (an inhibitor of MRE11) or NU7026 (an inhibitor of DNA-Pk). The number of biological replicates $n = 4$–5. (**C**) Ratio of the combined translocation frequencies of the two monocentric derivative chromosomes with respect to the combined translocation frequencies of the dicentric and acentric derivative chromosomes. The data are shown on a $\log_{10}$ scale. Translocations were induced in RPMI8866, Jurkat, K562, MRC5 and Hek-293 cells via electrotransfection with gRNA and Cas9 plasmids, targeting *MYC*, *IGH* and *AML* loci or *AML*, *ETO* and *IGH* loci and the resulting translocation frequencies were measured 2 days later by qPCR with a subset of primers that target monocentric (two pairs for each translocation), dicentric or acentric derivative chromosomes. Then, the frequencies of monocentric chromosomes were added and divided by the sum of frequencies of the dicentric and acentric derivative chromosomes, providing the resulting ratio. In almost all cases, the ratio was >1, indicating that the generation of monocentric derivative chromosomes was favored over dicentric and acentric ones. The number of biological replicates $n = 2$–7. (**D**, **E**) Frequencies of translocations induced by DSBs. RPMI8866, Jurkat, K562, MRC5 and Hek-293 cells were electrotransfected with gRNA and Cas9 plasmids, targeting MIA (D) or AEI (E). After 2 days, electrotransfected cells were collected for DNA extraction and translocations were detected using qPCR with translocation-specific PCR primers. The translocation frequencies were calculated as described in the 'Materials and Methods' section. Only the unicentric derivative chromosomes with the highest frequency compared to their reciprocal counterparts are shown in the graphs. Means ± standard errors of the mean (SEMs) of at least two biological and two technical replicates are shown. One-way ANOVA with Tukey's honest significant difference post-hoc test was performed to compare the translocation frequencies within each cell type: $^{**}P \leq 0.01$, $^{***}P \leq 0.001$ and $^{****}P \leq 0.0001$.

AML, *ETO* and *IGH* (AEI). DNA was collected 48 h later and all possible resulting translocations were quantified using qPCR as described in the 'Materials and Methods' section. In theory, each chromosome pair can form three types of translocations: unicentric (with one centromere; most cancer-related translocations are unicentric), dicentric (with two centromeres) and acentric (without centromeres). The latter two types of translocations are usually lost in the course of cell divisions; therefore, we concentrated on unicentric translocations.

In almost all translocations in all cell types, the combined translocation frequencies of the monocentric derivative chromosomes were higher compared to the combined dicentric and acentric derivative chromosomes after induction of three DSBs (Figure 1C), suggesting that the formation of monocentric derivative chromosomes is already favored early on. The *MYC–IGH* translocation had the highest frequency after MIA DSB induction (2–5 $\times$ 10^{-3} translocations/cell) compared to the *MYC–AML* and *AML–IGH* translocations (1–2 $\times$ 10^{-3} and 0.01–0.2 $\times$ 10^{-3} translocations/cell, respectively) (Figure 1D and Supplementary Figure S4A–E). After AEI DSB induction, the *ETO–IGH* translocation had the highest frequency (0.4–1 $\times$ 10^{-3} translocations/cell) compared to the *AML–IGH* and *AML–ETO* translocations (0.01–0.2 $\times$ 10^{-3} and 0.008–0.1 $\times$ 10^{-3} translocations/cell, respectively) (Figure 1E and Supplementary Figure S4F–J). Of the five cell types, Jurkat exhibited the highest translocation frequencies after induction of either MIA or AEI DSBs. The oncogenic *MYC–IGH* translocation had the highest frequency after MIA DSB induction (Figure 1D), while another oncogenic *AML–ETO* translocation had the lowest frequency after AEI DSB induction (Figure 1E), although it was relatively high in the myeloid K562 and epithelial Hek-293 cells (0.01 $\times$ 10^{-3} and 0.1 $\times$ 10^{-3}, respectively). Interestingly, the translocation frequencies involving the *MYC* locus were two to four times higher than those of the other translocations in all cell types. Another important conclusion is that while the studied cell lines had different ploidies, relative frequencies of translocations were similar across the cell lines with few exceptions.

Transcriptional activity and nuclear radial distribution of gene loci do not correlate with the translocation formation after DSB induction

We next tried to identify factors that could account for the observed translocation frequencies. Actively transcribed loci, loci with an open chromatin configuration or loci located close to each other may have higher propensities to form translocations (36–39). *MYC–IGH* and *AML–ETO* translocations will now serve as examples of our results, but all the described analyses were performed for all possible translocations.

We first correlated the frequencies of the *MYC–IGH* and *AML–ETO* translocations in different cell types (Figure 2A and B) with the transcriptional activity of the involved genes determined by quantitative reverse transcription PCR (Figure 2C) and no positive correlation was observed ($R_s = 0.24$, Figure 2D). Higher transcriptional activity did not always mean higher translocation rate. For example, both *MYC* and *IGH* were actively transcribed in the RPMI8866 cells, and *IGH* was minimally or not transcribed in other cell types, but this did not affect the frequency of the *MYC–IGH* translocation that remained high. On the contrary, the *AML–ETO* translocation was generated at a very low frequency in K562 cells (Figure 2B) even though the *AML* and *ETO* genes were actively transcribed (Figure 2C). The *ETO–IGH* translocation in Jurkat was still generated (Figure 1E) though neither *ETO* nor *IGH* was actively transcribed (Figure 2C).

Radial positions reflect the localization of gene loci within the nucleus. Peripheral regions of the nucleus are often heterochromatin-rich and transcriptionally repressed, while central regions are transcriptionally active. We determined the nuclear radial positions of the four gene loci before the DSB induction using 3D-FISH. The *MYC*, *IGH*, *AML* and *ETO* loci were positioned near the center of the nucleus and had a roughly similar radial distribution before (Figure 2E) and after DSB induction (Figure 2F). Thus, this factor could not solely account for the variability of translocation frequencies between different gene loci across the studied cell lines in our system.

The breakage-first model accounts for translocation formation after DSB induction

As translocations are produced by NHEJ, a proximity-based mechanism (40), we next studied whether the loci involved in the translocations were proximal in the cell nuclei. We have measured the distance between fluorescent signals corresponding to the studied loci. As each 3D-FISH signal was ~1 μm in diameter, two signals were considered to be proximal (colocalized) when the distance between their centers was no more than 1 μm, since at this distance, spots partially or completely overlapped. The spatial proximity between the gene loci was expressed as the percentage of cells where the two loci were colocalized. Surprisingly, before the occurrence of DSB, we did not observe a positive correlation between gene proximity and translocation rate ($R_s = 0.32$; $P = 0.0331$) (Figure 3C). As DSBs are known to induce mobility of the damaged gene loci [reviewed in (41)], we also measured gene proximity after the DSB induction. We observed a significant increase of gene loci proximity after DSB induction in the case of *MYC–IGH* and *ETO–IGH* pairs in all considered cell types (Figure 3A and D, and Supplementary Figure S5A–F) and the translocations between these very gene loci were also the most frequent (Figure 3B and E). A representative image shows the positions of *MYC* and *IGH* loci before and after the DSB induction (Figure 3G). It is noteworthy that colocalization of gene loci was a predisposing factor for their translocation but did not necessarily mean that they were translocated (e.g. *AML–ETO* were colocalized in 4.4 ± 0.3% of RPMI8866 cells after DSBs, but no translocations between these loci were observed; Figure 3D and E). Overall, we observe colocalization between loci at a much higher rate than translocations; this shows that colocalization alone is not sufficient to induce translocations. The inverse is also true, as in the case of *MYC–AML* translocation, where the loci were not found to colocalize at a detectable rate and yet the translocation was still formed (Figure 3A and B). When we took into

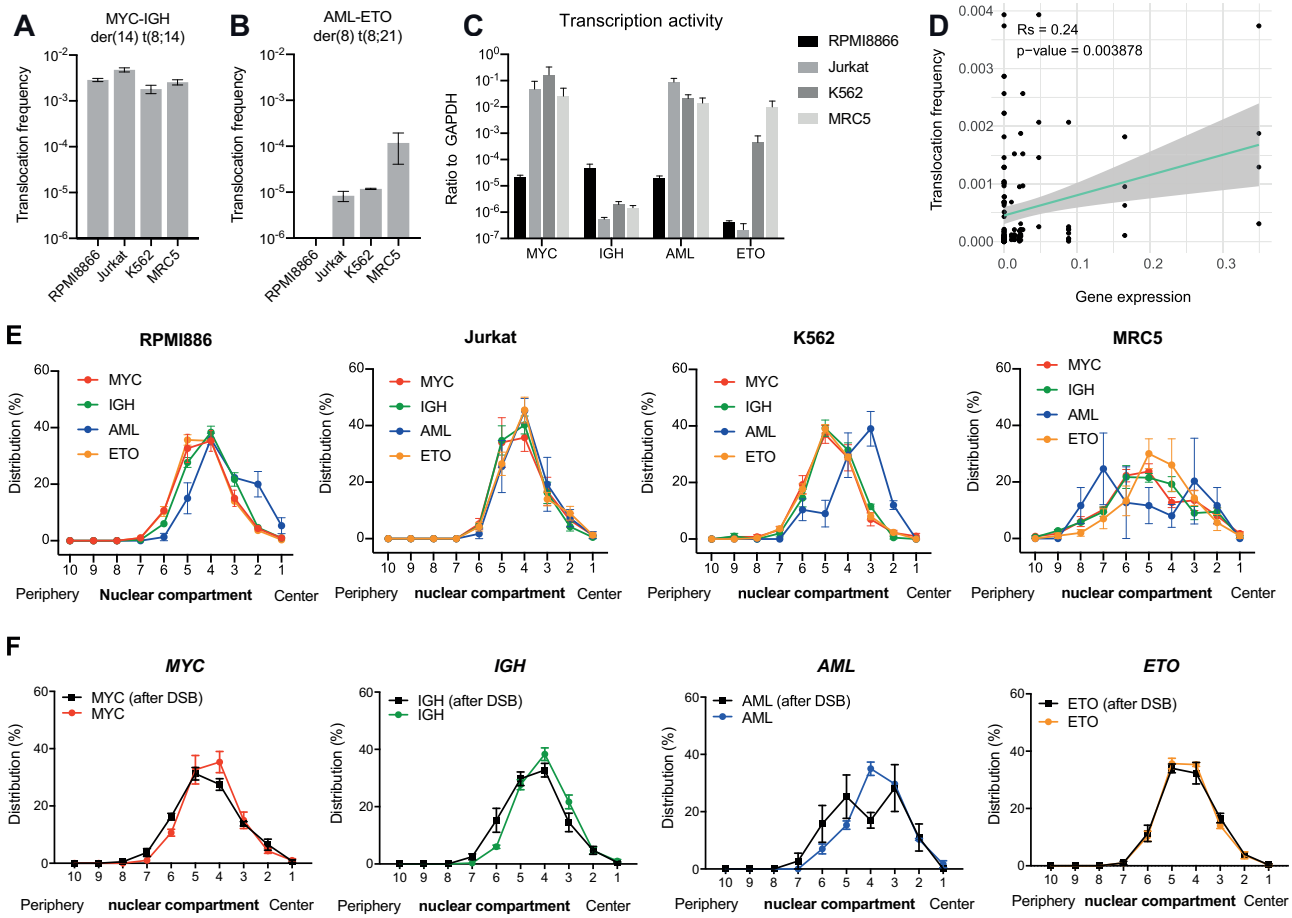

Figure 2. Transcriptional activity and nuclear radial position of gene loci do not correlate with their translocation frequency. Frequencies of the *MYC–IGH* (**A**) and *AML–ETO* (**B**) translocations across the cell lines. RPMI8866, Jurkat, K562 and MRC5 cells were electrotransfected with gRNAs and Cas9 plasmids targeting MIA (A) or AEI (B). Forty-eight hours after electrotransfection, cells were collected for DNA extraction and translocations were detected using qPCR with translocation-specific PCR primers. The translocation frequencies were calculated. Means ± SEMs are shown representing the results of two to four biological and two technical replicates. (**C**) Transcriptional activity of the *MYC*, *IGH, AML* and *ETO* genes in the studied cell lines. RNA was extracted from cells and relative fold gene expression with respect to the housekeeping gene *GAPDH* was calculated from Ct values obtained from the qPCR results as described in the 'Materials and Methods' section. Means ± SEMs of two to three biological and two technical replicates are shown. (**D**) Correlation plot for the gene expression and observed translocation frequencies. The Spearman correlation coefficient ($R_s = 0.24$) and its corresponding *P*-value (0.003878) are shown. The green line represents the linear regression fit and the gray area represents the 95% confidence intervals. (**E**) Radial position of the gene loci in the nuclear space of RPMI8866, Jurkat, K562 and MRC5 cells analyzed by 3D-FISH. (**F**) Radial position in the nuclear space of *MYC*, *IGH*, *AML* and *ETO* before and after DSB induction in RPMI8866. For the nuclear radial position before DSB induction, non-electrotransfected cells were collected and processed for 3D-FISH. For the nuclear radial position after DSB induction, RPMI8866 (16×10^6 cells) were electrotransfected with Cas9 and gRNA-expressing plasmids targeting either MIA or AEI. Two days after electrotransfection, cells were sorted for GFP, as the electrotransfected Cas9 plasmid also codes for GFP. The sorted cells were then processed for 3D-FISH. The images were acquired using a confocal microscope and analyzed using the Bitplane Imaris software. Each gene locus was mapped within the nucleus with respect to the 10 concentric compartments with the equal volume numbered from the center to the periphery of the nucleus. Data are presented as means ± SEMs of three to four biological replicates. For each technical replicate, at least 100 cells were analyzed.

consideration all detected translocations in all studied cell types, we could reveal a positive correlation ($R_s = 0.55$; $P = 0.0001$) between the proximity after the DSB and the translocation frequency (Figure 3F), indicating that translocation formation was affected by the spatial proximity between gene loci after the DSB induction. In multiple linear regression of different factors that could affect translocation frequency, which also took into account the cell type, only the proximity after the DSB showed a significant association with the translocation frequency ($P = 0.012$, Table 1).

To identify factors that affected loci movement after DSB induction, we used several inhibitors: NU7026 (an inhibitor of DNA-Pk), L67 (a DNA ligase I and III inhibitor) and KU-55933 (ATM inhibitor). We found that loci proximity after the DSB induction increased significantly in the presence of NU7026 (Figure 3H), which indicates that DNA-Pk-dependent signaling prevents loci relocation upon DSB.

Different survival outcomes of cells with chromosomal translocations

Our results show that any translocation can potentially arise in all types of cells; at the same time, the majority of described cancer-related chromosomal translocations

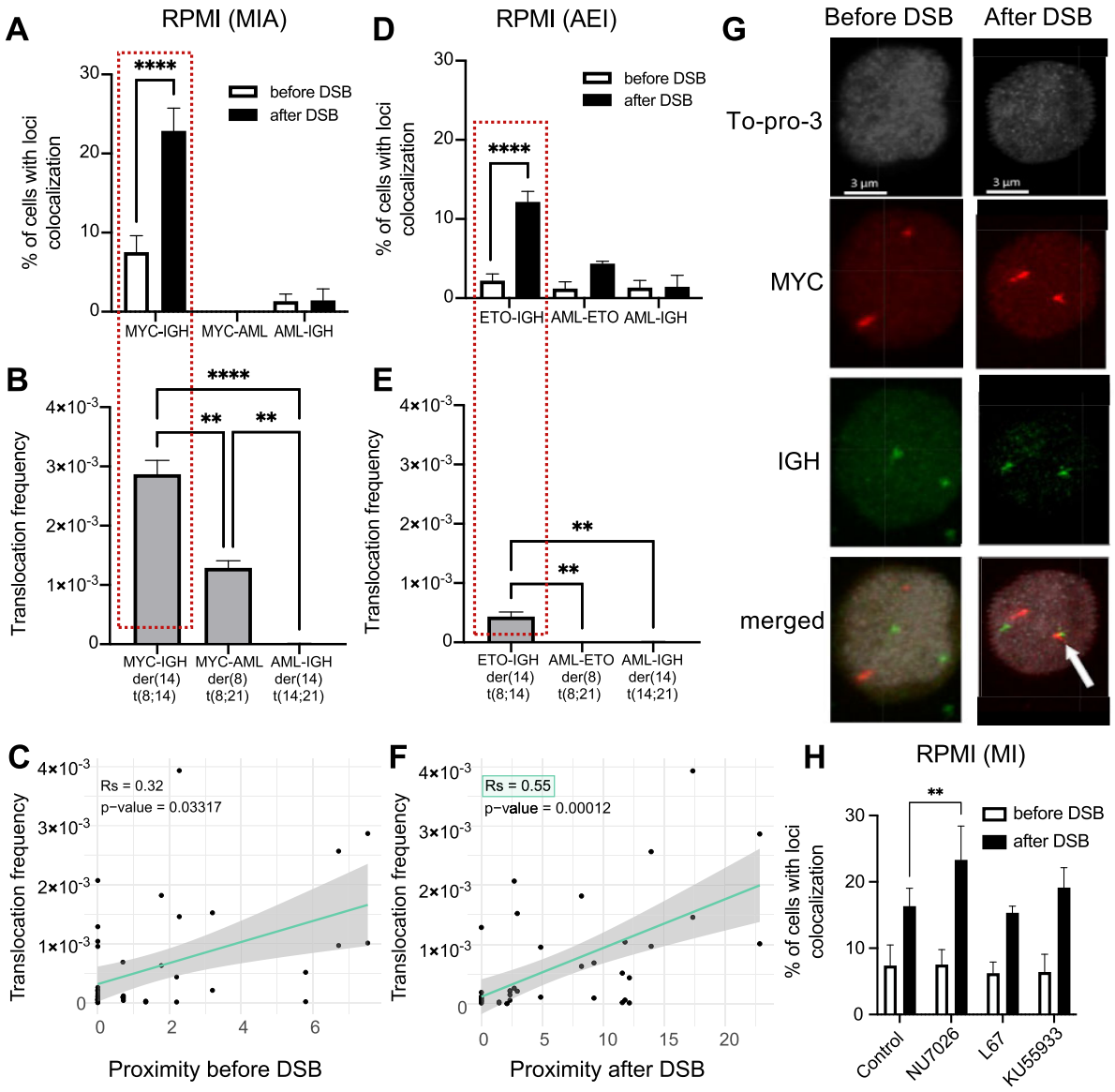

Figure 3. Spatial proximity between gene loci before and after DSB induction in RPMI8866. Spatial proximity between gene loci before and after DSB induction in MIA (**A**) and AEI (**D**) in RPMI8866. Non-electrotransfected cells (1–2 × 10^5) (before DSB) and sorted cells (after DSB) (1–2 × 10^5) that were electrotransfected with gRNAs and Cas9 plasmids 2 days prior were collected and processed for 3D-FISH. The slides were scanned using a confocal microscope and 3D-FISH images were analyzed in Bitplane Imaris software. The percentage of cells with the target gene loci pair located at 1 µm or less (colocalized) was calculated. The number of replicates $n = 2$–8. Translocation frequencies after DSB induction in MIA (**B**) and AEI (**E**) in RPMI8866. Only the unicentric derivative chromosomes with the highest frequency are shown. The number of replicates $n = 3$. Scatter plots of translocation frequency versus before DSB proximity (**C**) and after DSB proximity (**F**). The Spearman correlation coefficient (Rs) and its corresponding *P*-value are shown. (**G**) Representative 3D-FISH image of RPMI8866 cells before (left column) and after DSB induction (right column). The nuclei were stained with To-Pro-3 and are represented in the images as gray. Meanwhile, the *MYC* and *IGH* loci were stained with specific fluorescent probes and are represented in red and green, respectively. Colocalization between *MYC* and *IGH* is pointed out in the merged image by a white arrow. Scale bar = 3 µm. (**H**) Spatial proximity between gene loci before and after DSB induction in *MYC* and *IGH* (MI) in RPMI8866; cells were treated with NU7026 (an inhibitor of DNA-Pk), L67 (a DNA ligase I and III inhibitor), KU-55933 (ATM inhibitor) or left untreated (control). The number of replicates $n = 3$–7. For each replicate, at least 100 cells were analyzed. For all plotted values of each graph, one-way ANOVA was performed. For each comparison, the statistical significance is shown: $^{**}P \leq 0.01$ and $^{****}P \leq 0.0001$.

Table 1. Multiple linear regression of different factors involved in translocation formation. *P*-value < 0.05 is denoted in bold

	Translocation frequency		
Predictors	Estimates	95% CI	*P*-value
Cell type			
Jurkat	−0.00	−0.07 to 0.06	0.968
K562	−0.03	−0.10 to 0.04	0.385
MRC5	0.00	−0.05 to 0.06	0.869
RPMI8866	−0.01	−0.06 to 0.04	0.620
Loci proximity before DSB	0.00	−0.01 to 0.02	0.586
Loci proximity after DSB	0.01	0.00–0.01	**0.012**
Gene 1 expression	0.33	−0.24 to 0.89	0.251
Gene 2 expression	0.89	−0.36 to 2.14	0.156

Number of observations = 44; $R^2/R^2_{adjusted} = 0.621/0.537$; genes 1 and 2, genes involved in chromosomal translocation; 95% CI, 95% confidence intervals.

are cell type specific (3,42). This may be due to the selective advantage the translocation provides to only specific types of cells. To test this, we analyzed how the generated chromosomal translocations would be retained in different cell lines upon long-term culture. Cells transfected with CRISPR/Cas9 and gRNAs were cultured for 60 days with regular weekly passages. Translocation persistence was different in different cell types (Figure 4A–E and Supplementary Figure S6A–J). The proportion of cells bearing *MYC–IGH* translocation increased >50 times on Day 60 and attained over 10% of the total cell population as compared to Day 2 in RPMI8866 cells suggesting that *MYC–IGH* translocation could be a subject of positive selection in RPMI8866 cells. In other cell lines, *MYC–IGH* translocation either did not increase significantly or eventually decreased by Day 60. It should be noted that *IGH* is actively transcribed only in B cells and its translocation with *MYC* can lead to *MYC* overexpression in B cells (43). In addition, *MYC* expression was much lower in RPMI8866 cells prior to translocations as compared to other cell types (Figure 2C). On the other hand, the *AML–ETO* translocation was found to persist after long-term culture in MRC5 cells only (Supplementary Figure S6F–J) although still at a low frequency. These results point out that the generated chromosomal translocations either confer cell type-dependent survival advantages or are progressively eliminated from the cell population.

DISCUSSION

Why are certain chromosomal translocations observed in specific cell types? Several studies addressed this question before. They found that genes that are proximally positioned in the nuclear space, have a higher transcriptional activity or have an accessible chromatin configuration tend to have a higher propensity to form translocations in a specific cell type (22,44–52). Initial studies on chromosomal translocation formation utilized naturally occurring chromosomal translocations, as in the case of B-cell lymphomas, and then correlated their formation with the nuclear spatial position and transcription activity of the involved genes in normal cells (44,45). Naturally occurring chromosomal translocations are, however, significantly dependent on DSBs that occur in specific gene loci in these cells. More recently, stimulated chromosomal translocations were investigated after experimental induction of DSBs, either by programmed nucleases or by ionizing radiation. The resulting chromosomal translocations were tracked using live cell microscopy to characterize the spatial and dynamic properties of translocation formation (46). Variants of massively parallel sequencing (47,48) in combination with chromosome capture techniques (4C or Hi-C) (49–52) were also used to detect the generated translocations genome-wide to demonstrate the role of spatial proximity between gene loci and DSBs, gene transcription activity, chromatin configuration and nuclear organization in translocation formation. From these studies, the factors that appear to contribute significantly to translocation formation are the spatial proximity between the gene loci and their transcription activity (46–49,51). Translocation breakpoints were also found to be close to the transcription start sites (47–49).

Chromosomal translocations are products of erroneous repair of DSBs (9,53). The error-prone NHEJ repair pathway illegitimately joins two broken chromosomal ends from nonhomologous chromosomes (54). As NHEJ is a proximity-based repair, the physical proximity of the partner loci is a prerequisite to translocation formation (37). In this context, two models are proposed to explain the formation of chromosomal translocations (55). The 'contact-first' model proposes that the broken chromosomal ends are immobile or have limited movement in the nuclear space and that translocation occurs to those that are initially close to each other (colocalize prior to and at the time of DSB) (55). This is supported by the occurrence of chromosomal translocations involving gene loci that were already proximal, such as *RET* and *H4* (56), *ABL* and *BCR* (57), and *PML* and *RARA* (58) loci, or gene loci that have moved closer to each other before the chromosomal breakage occurred, e.g. *MYC* and *IGH* loci upon B-lymphocyte activation (18,22,44,45,59). The 'breakage-first' model postulates that broken chromosomal ends can freely move around the nuclear space and that the meeting of the two ends may lead to translocation formation. In this scenario, there is a higher likelihood for translocation to occur if DSB movement and colocalization increase. This DSB movement can be directed, stochastic or both [reviewed in (41)]. DSB mobility was observed in the case of multiple DSBs induced by alpha particles or ionizing radiation (60,61).

To experimentally test these conclusions, we induced several DSBs in specific loci of one cell and compared the frequency of resulting chromosomal translocations between these loci in different cell types using the CRISPR/Cas9 system (Figure 1). The advantage of this system is that CRISPR/Cas9 induces DSBs in both euchromatin and heterochromatin regions (although Cas9 can be less efficient in heterochromatin regions) (23,24,26,27). Additionally, the repair of DSBs after Cas9 cleavage is error-prone, which prevents recutting of the same locus (62). The observed translocations were likely produced by the alternative NHEJ pathway as inhibition of DNA-Pk, an important component of the canonical NHEJ, resulted in a significant increase of translocation frequency (Figure 1B). This result is in agreement with previous studies that reported that in rodent and human cells chromosome

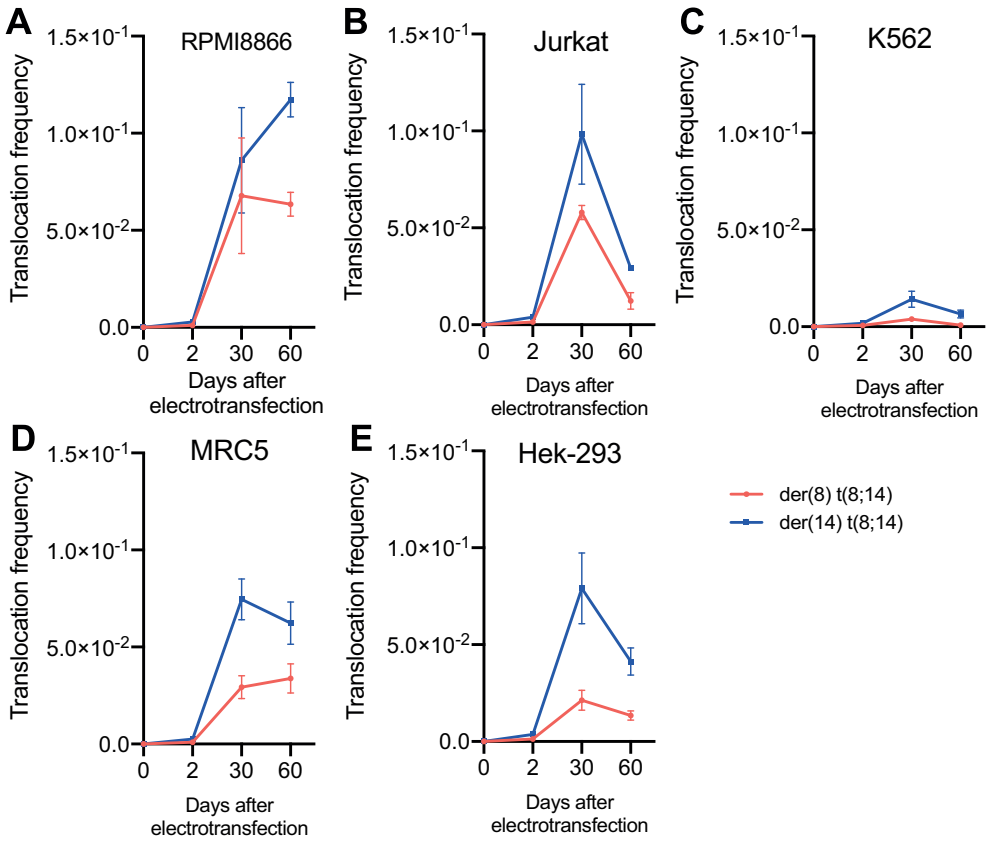

Figure 4. *MYC–IGH* translocation frequency after long-term culture. RPMI8866 (**A**), Jurkat (**B**), K562 (**C**), MRC5 (**D**) and Hek-293 (**E**) cells (24–32 × 10^6) were electrotransfected with gRNA, targeting *MYC, IGH* and *AML*, and Cas9 plasmids. Two days later, the electrotransfected cells were split into two parts. The first part was collected to determine the *MYC–IGH* translocation frequency. The second part was sorted and then cultured for 60 days with regular weekly passage. Cells were collected 30 and 60 days after electrotransfection to determine the *MYC–IGH* translocation frequency. Both of the reciprocal (der8, red line; der14, blue line) *MYC–IGH* translocations are shown. Data represent means ± SEMs of two independent biological experiments and two technical replicates.

translocations are mainly formed by the alternative NHEJ pathway (46,63–67). Nonetheless, a subset of chromosomal translocations may be generated through the canonical NHEJ pathway (68,69). The increased frequency of translocations when canonical NHEJ is abrogated can be explained by the slow kinetics of DNA repair via alternative NHEJ, which is ∼10-fold slower than canonical NHEJ; this permits the free movement of unrepaired DNA ends, increasing the chance to meet their translocation partner in the nuclear space (70). Likewise, we observed that inhibiting DNA-Pk increased *MYC–IGH* colocalization after the DSB (Figure 3H). The accumulation of DSB clustering upon DNA-Pk inhibition was also recently described by Zagelbaum *et al.* (68).

Interestingly, all possible combinations of translocations can be generated in almost any cell type, albeit with different frequencies (Supplementary Figure S4A–J), although the generation of monocentric derivative chromosomes was favored over dicentric and acentric ones (Figure 1C). The mechanism of this preferential formation of unicentric derivative chromosomes early after DNA repair deserves a separate study. It can be noted that *MYC–IGH* translocation frequency was higher compared to the *MYC–AML* translocation frequency in all cell lines (Figure 1D), while the ratio of monocentric versus dicentric and acentric chromosomes was much lower for *MYC–IGH* compared to *MYC–AML* in these cells (Figure 1C). From these data, it seems that pro-oncogenic *MYC* and *IGH* breaks tend to be 'incorrectly' repaired to a greater extent than others, i.e. more often form translocated and dicentric/acentric derivatives. We hypothesize that the DSB in *IGH* loci, located in the subtelomeric region of chromosome 14, produces a relatively small and motile chromosomal fragment of 1 Mb that can migrate larger distances more readily to meet its translocation partner compared to a larger *AML* fragment (12 Mb): both *MYC–IGH* (t8;14) and *ETO–IGH* (t8;14) translocation frequencies are higher than *MYC–AML* (t8;21) and *ETO–AML* (t8;21) translocation frequencies (Figure 1D and Supplementary Figure S1E).

The cell lines that we used were diploid, except for K562 (nearly triploid) and Hek-293 (hypotriploid). Although the cell lines had different numbers of induced DSBs, the resulting translocation frequency profiles were similar among them (Table 1), indicating that the ploidy did not play a significant role in the pattern of chromosomal translocations after simultaneous induction of DSBs.

Once DSBs are formed, shared transcription factories (71), as well as spatial positioning (72), are the potential factors influencing DSB repair and thus they could affect translocation frequency. In our system, however, the frequency of translocations was not affected by the nuclear radial position or transcription activity of the participating gene loci (Figure 2 and Table 1), but rather by their spatial proximity after the DSB induction (Figure 3 and Table 1). This favors the 'breakage-first' hypothesis of translocation formation. An increase in *MYC–IGH* and *ETO–IGH* colocalization frequencies, but not in *MYC–AML* or *ETO–AML* colocalization frequencies, after the respective DSBs (Figure 3A and D) corroborates the higher motility of a shorter chromosomal fragment (*IGH*) proposed above. Different loci, however, may behave differently regarding translocation frequency and colocalization after DSB induction; e.g. colocalizing *AML* and *ETO* loci did not translocate in RPMI8866 cells (Figure 3D and E), while *MYC* and *AML* were not found to colocalize at a detectable rate and yet the translocation was still formed (Figure 3A and B). The mobility of DSBs was previously described (41,61,73), and it may serve either to facilitate the search of a recombination partner (39,74) or to join common DNA repair centers (60,75). DSBs were found to cluster in DNA damage repair foci in yeasts and mammalian cells (60,75,76). However, in mammalian cells DSB clustering was mostly observed for multiple DSBs (67,68,75). An increase in chromatin movement following DSBs can result in chromosomal translocations (46).

Regarding the role of transcription, it is important to acknowledge that while we observe no significant positive correlation between basal transcriptional activity and translocation frequency in between cell line comparisons, this may not concern the changes in gene expression within one cell line and their potential influence on translocation frequency. Whether changes in gene transcriptional activity or distance from DSB to transcription start sites might affect translocation frequencies requires further exploration. Similarly, while our data did not show a significant effect of nuclear radial position on translocation frequency, we acknowledge that this may be influenced by other factors and may vary depending on the specific loci and cell types.

We next tested the persistence of the observed chromosomal translocations upon long-term culture and found that it was different in different cell types (Figure 4A–E and Supplementary Figure S6A–J). Two months after DSB induction, the proportion of cells bearing *MYC–IGH* translocation continued to increase only in RPMI8866 cells (Figure 4A), while the *AML–ETO* translocation was found to persist after long-term culture in MRC5 cells only (Supplementary Figure S6I). These results point out that the generated oncogenic chromosomal translocations confer cell type-dependent survival advantages. The persistence of chromosomal translocations may also depend on whether both derivative chromosomes are present and no genetic material is lost. That is what we supposedly observed in the case of the *MYC–IGH* translocation in RPMI8866 cells, where both derivative chromosomes were present (Figure 4A). A more precise evaluation of potential genetic material loss during such selection requires further investigation. This finding adds to the ongoing discussion on the role of selection in the formation of cancer cells (77) and provides new evidence for the importance of considering the selective survival advantage of chromosomal translocations in different cell types.

We should also mention the limitations of our system, which provides a valid approximation but does not fully recapitulate all aspects of natural carcinogenesis in primary cells. With CRISPR/Cas9, we deliberately create several simultaneous DSBs; however, 'naturally occurring' DSBs can arise spontaneously and not necessarily at the same time, and their origins are diverse, encompassing external factors, e.g. irradiation, and various cellular activities, such as gene transcription, DNA replication and oxidative metabolism (31). Certain chromosomal translocations are caused by DNA-damaging enzymes (RAGs, AID, topoisomerases I and II). These enzymes are sensitive to chromatin organization, transcription and/or DNA sequence. Other chromosomal translocations are induced by random factors that are less strongly dependent on the chromatin context. These include ionizing radiation, oxidative stress, etc. As CRISPR/Cas9 is less sensitive to chromatin structure, it better reproduces the latter situation, although this does not invalidate our conclusions on translocation formation. A potential contributor to the choice of repair pathway, and thus translocation formation, is the cell cycle (78,79), which was not directly addressed in the current study. Further use of our experimental model will allow us to unravel other patterns in the generation of chromosomal translocations. The results on the persistence of the observed chromosomal translocations upon long-term culture might be limited by the fact that we used already proliferating cells; thus, the potential survival or growth rate advantages of chromosomal translocations on different cell types might not be fully estimated.

To conclude, we devised an experimental system to study the factors that drive the formation of chromosomal translocations between four distinct gene loci and five cell types; all the possible combinations of translocations can be generated in almost any cell type, albeit with different frequencies. The frequency of translocations correlates only with the spatial proximity of the partner loci after the DSB induction supporting the 'breakage-first' model for translocation formation. Upon long-term culture, only oncogenic *MYC–IGH* and *AML–ETO* chromosomal translocations conferred cell type-dependent survival advantages.

DATA AVAILABILITY

The data underlying this article are available in the article and in its online supplementary material.

SUPPLEMENTARY DATA

Supplementary Data are available at NAR Cancer Online.

ACKNOWLEDGEMENTS

The authors express their gratitude to Tudor Manoliu and Yann Lecluse, Gustave Roussy Cancer Campus, Plateforme Imagerie et Cytométrie—UMS 23/3655—Université Paris Saclay, Villejuif, France, for their technical help.

Authors' contributions: R.J.C. performed the experiments, analyzed and interpreted data, and wrote the original draft; A.S. and A.K. performed the experiments, analyzed and interpreted data, and wrote the paper (review and editing); N.L., E.T., Y.K. and F.A. performed the experiments; D.G. and Y.V. designed research, analyzed data and wrote the paper (review and editing). All authors read and approved the final manuscript.

FUNDING

Ministry of Science and Higher Education of the Russian Federation [075-15-2020-773]; CHED-PhilFrance Scholarship Programme (to R.J.C.).

Conflict of interest statement. The authors declare that they have no conflict of interest.

REFERENCES

1. Wilch,E.S. and Morton,C.C. (2018) Historical and clinical perspectives on chromosomal translocations. In: Zhang,Y. (ed). *Advances in Experimental Medicine and Biology*. Springer, Singapore, pp. 1–14.
2. Lobato,M.N., Metzler,M., Drynan,L., Forster,A., Pannell,R. and Rabbitts,T.H. (2008) Modeling chromosomal translocations using conditional alleles to recapitulate initiating events in human leukemias. *JNCI Monogr.*, **2008**, 58–63.
3. Mitelman,F., Johansson,B. and Mertens,F. (2021) In: *Mitelman Database of Chromosome Aberrations and Gene Fusions in Cancer*. https://mitelmandatabase.isb-cgc.org.
4. Nakano,K. and Takahashi,S. (2018) Translocation-related sarcomas. *Int. J. Mol. Sci.*, **19**, 3784.
5. Nambiar,M. and Raghavan,S.C. (2011) How does DNA break during chromosomal translocations?*Nucleic Acids Res.*, **39**, 5813–5825.
6. Bohlander,S.K., Kakadiya,P.M. and Coysh,A. (2019) Chromosome rearrangements and translocations. In: Boffetta, P. and Hainaut,P. (eds.) *Encyclopedia of Cancer*, 3rd edn. Academic Press, Oxford, pp. 389–404.
7. Pannunzio,N.R. and Lieber,M.R. (2018) Concept of DNA lesion longevity and chromosomal translocations. *Trends Biochem. Sci.*, **43**, 490–498.
8. Zheng,H. and Xie,W. (2019) The role of 3D genome organization in development and cell differentiation. *Nat. Rev. Mol. Cell Biol.*, **20**, 535–550.
9. Canoy,R.J., Shmakova,A., Karpukhina,A., Shepelev,M., Germini,D. and Vassetzky,Y. (2022) Factors that affect the formation of chromosomal translocations in cells. *Cancers*, **14**, 5110.
10. Lieber,M.R. (2010) The mechanism of double-strand DNA break repair by the nonhomologous DNA end-joining pathway. *Annu. Rev. Biochem.*, **79**, 181–211.
11. Liu,M., Duke,J.L., Richter,D.J., Vinuesa,C.G., Goodnow,C.C., Kleinstein,S.H. and Schatz,D.G. (2008) Two levels of protection for the B cell genome during somatic hypermutation. *Nature*, **451**, 841–845.
12. Shmakova,A. and Vassetzky,Y. (2023) lncRNA: a new danger for genome integrity. *Int. J. Cancer*, **152**, 1288–1289.
13. Demin,D.E., Murashko,M.M., Uvarova,A.N., Stasevich,E.M., Shyrokova,E.Y., Gorlachev,G.E., Zaretsky,A., Korneev,K.V., Ustiugova,A.S., Tkachenko,E.A. *et al.* (2023) Adversary of DNA integrity: a long non-coding RNA stimulates driver oncogenic chromosomal rearrangement in human thyroid cells. *Int. J. Cancer*, **152**, 1452–1462.
14. Shmakova,A.A., Lomov,N., Viushkov,V., Tsfasman,T., Kozhevnikova,Y., Sokolova,D., Pokrovsky,V., Syrkina,M., Germini,D., Rubtsov,M. *et al.* (2023) Cell models with inducible oncogenic translocations allow to evaluate the potential of drugs to favor secondary translocations. *Cancer Commun.*, **43**, 154–158.
15. Kovalchuk,A.L., Ansarah-Sobrinho,C., Hakim,O., Resch,W., Tolarová,H., Dubois,W., Yamane,A., Takizawa,M., Klein,I., Hager,G.L. *et al.* (2012) Mouse model of endemic Burkitt translocations reveals the long-range boundaries of Ig-mediated oncogene deregulation. *Proc. Natl Acad. Sci. U.S.A.*, **109**, 10972–10977.
16. Busch,K., Keller,T., Fuchs,U., Yeh,R.-F., Harbott,J., Klose,I., Wiemels,J., Novosel,A., Reiter,A. and Borkhardt,A. (2007) Identification of two distinct MYC breakpoint clusters and their association with various IGH breakpoint regions in the t(8;14) translocations in sporadic Burkitt-lymphoma. *Leukemia*, **21**, 1739–1751.
17. Brunet,E., Simsek,D., Tomishima,M., DeKelver,R., Choi,V.M., Gregory,P., Urnov,F., Weinstock,D.M. and Jasin,M. (2009) Chromosomal translocations induced at specified loci in human stem cells. *Proc. Natl Acad. Sci. U.S.A.*, **106**, 10620–10625.
18. Germini,D., Tsfasman,T., Klibi,M., El-Amine,R., Pichugin,A., Iarovaia,O.V., Bilhou-Nabera,C., Subra,F., Bou Saada,Y., Sukhanova,A. *et al.* (2017) HIV Tat induces a prolonged MYC relocalization next to IGH in circulating B-cells. *Leukemia*, **31**, 2515–2522.
19. Piganeau,M., Ghezraoui,H., De Cian,A., Guittat,L., Tomishima,M., Perrouault,L., René,O., Katibah,G.E., Zhang,L., Holmes,M.C. *et al.* (2013) Cancer translocations in human cells induced by zinc finger and TALE nucleases. *Genome Res.*, **23**, 1182–1193.
20. Vanoli,F. and Jasin,M. (2017) Generation of chromosomal translocations that lead to conditional fusion protein expression using CRISPR–Cas9 and homology-directed repair. *Methods*, **121–122**, 138–145.
21. Vanoli,F., Tomishima,M., Feng,W., Lamribet,K., Babin,L., Brunet,E. and Jasin,M. (2017) CRISPR–Cas9-guided oncogenic chromosomal translocations with conditional fusion protein expression in human mesenchymal cells. *Proc. Natl Acad. Sci. U.S.A.*, **114**, 3696–3701.
22. Sall,F.B., Shmakova,A., Karpukhina,A., Tsfasman,T., Lomov,N., Canoy,R.J., Boutboul,D., Oksenhendler,E., Toure,A.O., Lipinski,M. *et al.* (2023) Epstein–Barr virus reactivation induces MYC–IGH spatial proximity and t(8;14) in B cells. *J. Med. Virol.*, **95**, e28633.
23. Jain,S., Shukla,S., Yang,C., Zhang,M., Fatma,Z., Lingamaneni,M., Abesteh,S., Lane,S.T., Xiong,X., Wang,Y. *et al.* (2021) TALEN outperforms Cas9 in editing heterochromatin target sites. *Nat. Commun.*, **12**, 606.
24. Mitrentsi,I. and Soutoglou,E. (2021) CRISPR/Cas9-induced breaks in heterochromatin, visualized by immunofluorescence. *Methods Mol. Biol.*, **2153**, 439–445.
25. Schep,R., Brinkman,E.K., Leemans,C., Vergara,X., van der Weide,R.H., Morris,B., van Schaik,T., Manzo,S.G., Peric-Hupkes,D., van den Berg,J. *et al.* (2021) Impact of chromatin context on Cas9-induced DNA double-strand break repair pathway balance. *Mol. Cell*, **81**, 2216–2230.
26. Kallimasioti-Pazi,E.M., Thelakkad Chathoth,K., Taylor,G.C., Meynert,A., Ballinger,T., Kelder,M.J.E., Lalevée,S., Sanli,I., Feil,R. and Wood,A.J. (2018) Heterochromatin delays CRISPR–Cas9 mutagenesis but does not influence the outcome of mutagenic DNA repair. *PLoS Biol.*, **16**, e2005595.
27. Friskes,A., Koob,L., Krenning,L., Severson,T.M., Koeleman,E.S., Vergara,X., Schubert,M., van den Berg,J., Evers,B., Manjón,A.G. *et al.* (2022) Double-strand break toxicity is chromatin context independent. *Nucleic Acids Res.*, **50**, 9930–9947.
28. Concordet,J.-P. and Haeussler,M. (2018) CRISPOR: intuitive guide selection for CRISPR/Cas9 genome editing experiments and screens. *Nucleic Acids Res.*, **46**, W242–W245.
29. Brinkman,E.K., Chen,T., Amendola,M. and Van Steensel,B. (2014) Easy quantitative assessment of genome editing by sequence trace decomposition. *Nucleic Acids Res.*, **42**, e168.
30. Germini,D., Saada,Y.B., Tsfasman,T., Osina,K., Robin,C., Lomov,N., Rubtsov,M., Sjakste,N., Lipinski,M. and Vassetzky,Y. (2017) A one-step PCR-based assay to evaluate the efficiency and precision of genomic DNA-editing tools. *Mol. Ther. Methods Clin. Dev.*, **5**, 43–50.
31. Canoy,R.J., André,F., Shmakova,A., Wiels,J., Lipinski,M., Vassetzky,Y. and Germini,D. (2023) Easy and robust electrotransfection protocol for efficient ectopic gene expression and genome editing in human B cells. *Gene Ther.*, **30**, 167–171.
32. Akbay,B., Germini,D., Bissenbaev,A.K., Musinova,Y.R., Sheval,E.V., Vassetzky,Y. and Dokudovskaya,S. (2021) HIV-1 Tat activates Akt/mTORC1 pathway and AICDA expression by

downregulating its transcriptional inhibitors in B cells. *Int. J. Mol. Sci.*, **22**, 1588.
33. Pfaffl,M.W. (2001) A new mathematical model for relative quantification in real-time RT-PCR. *Nucleic Acids Res.*, **29**, e45.
34. Brunet,E. and Jasin,M. (2018) Induction of chromosomal translocations with CRISPR–Cas9 and other nucleases: understanding the repair mechanisms that give rise to translocations. In: Zhang,Y. (ed.) *Chromosome Translocation, Advances in Experimental Medicine and Biology*. Springer, Singapore, pp. 15–25.
35. Naumann,S., Reutzel,D., Speicher,M. and Decker,H.J. (2001) Complete karyotype characterization of the K562 cell line by combined application of G-banding, multiplex-fluorescence *in situ* hybridization, fluorescence *in situ* hybridization, and comparative genomic hybridization. *Leuk. Res.*, **25**, 313–322.
36. Lin,C.-Y., Shukla,A., Grady,J.P., Fink,J.L., Dray,E. and Duijf,P.H.G. (2018) Translocation breakpoints preferentially occur in euchromatin and acrocentric chromosomes. *Cancers*, **10**, 13.
37. Misteli,T. (2010) Higher-order genome organization in human disease. *Cold Spring Harb. Perspect. Biol.*, **2**, a000794.
38. Osborne,C.S. (2014) Molecular pathways: transcription factories and chromosomal translocations. *Clin. Cancer Res.*, **20**, 296–300.
39. Miné-Hattab,J. and Chiolo,I. (2020) Complex chromatin motions for DNA repair. *Front. Genet.*, **11**, 800.
40. Pannunzio,N.R., Watanabe,G. and Lieber,M.R. (2018) Nonhomologous DNA end-joining for repair of DNA double-strand breaks. *J. Biol. Chem.*, **293**, 10512–10523.
41. Iarovaia,O.V., Rubtsov,M., Ioudinkova,E., Tsfasman,T., Razin,S.V. and Vassetzky,Y.S. (2014) Dynamics of double strand breaks and chromosomal translocations. *Mol. Cancer*, **13**, 249.
42. Mitelman,F., Johansson,B. and Mertens,F. (2007) The impact of translocations and gene fusions on cancer causation. *Nat. Rev. Cancer*, **7**, 233–245.
43. Saleh,K., Michot,J.-M., Camara-Clayette,V., Vassetsky,Y. and Ribrag,V. (2020) Burkitt and Burkitt-like lymphomas: a systematic review. *Curr. Oncol. Rep.*, **22**, 33.
44. Osborne,C.S., Chakalova,L., Mitchell,J.A., Horton,A., Wood,A.L., Bolland,D.J., Corcoran,A.E. and Fraser,P. (2007) Myc dynamically and preferentially relocates to a transcription factory occupied by Igh. *PLoS Biol.*, **5**, e192.
45. Roix,J.J., McQueen,P.G., Munson,P.J., Parada,L.A. and Misteli,T. (2003) Spatial proximity of translocation-prone gene loci in human lymphomas. *Nat. Genet.*, **34**, 287–291.
46. Roukos,V., Voss,T.C., Schmidt,C.K., Lee,S., Wangsa,D. and Misteli,T. (2013) Spatial dynamics of chromosome translocations in living cells. *Science*, **341**, 660–664.
47. Chiarle,R., Zhang,Y., Frock,R.L., Lewis,S.M., Molinie,B., Ho,Y.-J., Myers,D.R., Choi,V.W., Compagno,M., Malkin,D.J. *et al.* (2011) Genome-wide translocation sequencing reveals mechanisms of chromosome breaks and rearrangements in B cells. *Cell*, **147**, 107–119.
48. Klein,I.A., Resch,W., Jankovic,M., Oliveira,T., Yamane,A., Nakahashi,H., Di Virgilio,M., Bothmer,A., Nussenzweig,A., Robbiani,D.F. *et al.* (2011) Translocation-capture sequencing reveals the extent and nature of chromosomal rearrangements in B lymphocytes. *Cell*, **147**, 95–106.
49. Hakim,O., Resch,W., Yamane,A., Klein,I., Kieffer-Kwon,K.-R., Jankovic,M., Oliveira,T., Bothmer,A., Voss,T.C., Ansarah-Sobrinho,C. *et al.* (2012) DNA damage defines sites of recurrent chromosomal translocations in B lymphocytes. *Nature*, **484**, 69–74.
50. Rocha,P.P., Micsinai,M., Kim,J.R., Hewitt,S.L., Souza,P.P., Trimarchi,T., Strino,F., Parisi,F., Kluger,Y. and Skok,J.A. (2012) Close proximity to Igh is a contributing factor to AID-mediated translocations. *Mol. Cell*, **47**, 873–885.
51. Zhang,Y., McCord,R.P., Ho,Y.-J., Lajoie,B.R., Hildebrand,D.G., Simon,A.C., Becker,M.S., Alt,F.W. and Dekker,J. (2012) Spatial organization of the mouse genome and its role in recurrent chromosomal translocations. *Cell*, **148**, 908–921.
52. Aymard,F., Aguirrebengoa,M., Guillou,E., Javierre,B.M., Bugler,B., Arnould,C., Rocher,V., Iacovoni,J.S., Biernacka,A., Skrzypczak,M. *et al.* (2017) Genome-wide mapping of long-range contacts unveils clustering of DNA double-strand breaks at damaged active genes. *Nat. Struct. Mol. Biol.*, **24**, 353–361.
53. Roukos,V. and Misteli,T. (2014) The biogenesis of chromosome translocations. *Nat. Cell Biol.*, **16**, 293–300.
54. Lieber,M.R., Gu,J., Lu,H., Shimazaki,N. and Tsai,A.G. (2010) Nonhomologous DNA end joining (NHEJ) and chromosomal translocations in humans. In: Nasheuer,H.-P. (ed). *Genome Stability and Human Diseases, Subcellular Biochemistry*. Springer Netherlands, Dordrecht, pp. 279–296.
55. Meaburn,K.J., Misteli,T. and Soutoglou,E. (2007) Spatial genome organization in the formation of chromosomal translocations. *Semin. Cancer Biol.*, **17**, 80–90.
56. Nikiforova,M.N., Stringer,J.R., Blough,R., Medvedovic,M., Fagin,J.A. and Nikiforov,Y.E. (2000) Proximity of chromosomal loci that participate in radiation-induced rearrangements in human cells. *Science*, **290**, 138–141.
57. Lukášová,E., Kozubek,S., Kozubek,M., Kjeronská,J., Rýznar,L., Horáková,J., Krahulcová,E. and Horneck,G. (1997) Localisation and distance between ABL and BCR genes in interphase nuclei of bone marrow cells of control donors and patients with chronic myeloid leukaemia. *Hum. Genet.*, **100**, 525–535.
58. Neves,H., Ramos,C., da Silva,M.G., Parreira,A. and Parreira,L. (1999) The nuclear topography of ABL, BCR, PML, and RARα genes: evidence for gene proximity in specific phases of the cell cycle and stages of hematopoietic differentiation. *Blood*, **93**, 1197–1207.
59. Boxer,L.M. and Dang,C.V. (2001) Translocations involving c-myc and c-myc function. *Oncogene*, **20**, 5595–5610.
60. Aten,J.A., Stap,J., Krawczyk,P.M., Oven,C.H., Hoebe,R.A., Essers,J. and Kanaar,R.. (2004) Dynamics of DNA double-strand breaks revealed by clustering of damaged chromosome domains. *Science*, **303**, 92–95.
61. Krawczyk,P.M., Borovski,T., Stap,J., Cijsouw,T., Cate,R., Medema,J.P., Kanaar,R., Franken,N.A.P. and Aten,J.A. (2012) Chromatin mobility is increased at sites of DNA double-strand breaks. *J. Cell Sci.*, **125**, 2127–2133.
62. Brinkman,E.K., Chen,T., de Haas,M., Holland,H.A., Akhtar,W. and van Steensel,B. (2018) Kinetics and fidelity of the repair of Cas9-induced double-strand DNA breaks. *Mol. Cell*, **70**, 801–813.e6.
63. Soni,A., Siemann,M., Pantelias,G.E. and Iliakis,G. (2015) Marked contribution of alternative end-joining to chromosome-translocation-formation by stochastically induced DNA double-strand-breaks in G2-phase human cells. *Mutat. Res. Genet. Toxicol. Environ. Mutagen.*, **793**, 2–8.
64. Zhang,Y. and Jasin,M. (2011) An essential role for CtIP in chromosomal translocation formation through an alternative end-joining pathway. *Nat. Struct. Mol. Biol.*, **18**, 80–84.
65. Boboila,C., Jankovic,M., Yan,C.T., Wang,J.H., Wesemann,D.R., Zhang,T., Fazeli,A., Feldman,L., Nussenzweig,A., Nussenzweig,M. *et al.* (2010) Alternative end-joining catalyzes robust IgH locus deletions and translocations in the combined absence of ligase 4 and Ku70. *Proc. Natl Acad. Sci. U.S.A.*, **107**, 3034–3039.
66. Simsek,D. and Jasin,M. (2010) Alternative end-joining is suppressed by the canonical NHEJ component Xrcc4–ligase IV during chromosomal translocation formation. *Nat. Struct. Mol. Biol.*, **17**, 410–416.
67. Caron,P., Choudjaye,J., Clouaire,T., Bugler,B., Daburon,V., Aguirrebengoa,M., Mangeat,T., Iacovoni,J.S., Álvarez-Quilón,A., Cortés-Ledesma,F. *et al.* (2015) Non-redundant functions of ATM and DNA-PKcs in response to DNA double-strand breaks. *Cell Rep.*, **13**, 1598–1609.
68. Zagelbaum,J., Schooley,A., Zhao,J., Schrank,B.R., Callen,E., Zha,S., Gottesman,M.E., Nussenzweig,A., Rabadan,R., Dekker,J. *et al.* (2023) Multiscale reorganization of the genome following DNA damage facilitates chromosome translocations via nuclear actin polymerization. *Nat. Struct. Mol. Biol.*, **30**, 99–106.
69. Ghezraoui,H., Piganeau,M., Renouf,B., Renaud,J. - B., Sallmyr,A., Ruis,B., Oh,S., Tomkinson,A.E., Hendrickson,E.A., Giovannangeli,C. *et al.* (2014) Chromosomal translocations in human cells are generated by canonical nonhomologous end-joining. *Mol. Cell*, **55**, 829–842.
70. Lieber,M.R. (2010) NHEJ and its backup pathways: relation to chromosomal translocations. *Nat. Struct. Mol. Biol.*, **17**, 393–395.
71. Osborne,C.S., Chakalova,L., Brown,K.E., Carter,D., Horton,A., Debrand,E., Goyenechea,B., Mitchell,J.A., Lopes,S., Reik,W. *et al.* (2004) Active genes dynamically colocalize to shared sites of ongoing transcription. *Nat. Genet.*, **36**, 1065–1071.

72. Tsouroula,K., Furst,A., Rogier,M., Heyer,V., Maglott-Roth,A., Ferrand,A., Reina-San-Martin,B. and Soutoglou,E. (2016) Temporal and spatial uncoupling of DNA double strand break repair pathways within mammalian heterochromatin. *Mol. Cell*, **63**, 293–305.
73. Kruhlak,M.J., Celeste,A., Dellaire,G., Fernandez-Capetillo,O., Müller,W.G., McNally,J.G., Bazett-Jones,D.P. and Nussenzweig,A. (2006) Changes in chromatin structure and mobility in living cells at sites of DNA double-strand breaks. *J. Cell Biol.*, **172**, 823–834.
74. Miné-Hattab,J. and Rothstein,R. (2012) Increased chromosome mobility facilitates homology search during recombination. *Nat. Cell Biol.*, **14**, 510–517.
75. Neumaier,T., Swenson,J., Pham,C., Polyzos,A., Lo,A.T., Yang,P., Dyball,J., Asaithamby,A., Chen,D.J., Bissell,M.J. *et al.* (2012) Evidence for formation of DNA repair centers and dose-response nonlinearity in human cells. *Proc. Natl Acad. Sci. U.S.A.*, **109**, 443–448.
76. Lisby,M., Rothstein,R. and Mortensen,U.H. (2001) Rad52 forms DNA repair and recombination centers during S phase. *Proc. Natl Acad. Sci. U.S.A.*, **98**, 8276–8282.
77. Vendramin,R., Litchfield,K. and Swanton,C. (2021) Cancer evolution: Darwin and beyond. *EMBO J.*, **40**, e108389.
78. Jasin,M. and Rothstein,R. (2013) Repair of strand breaks by homologous recombination. *Cold Spring Harb. Perspect. Biol.*, **5**, a012740.
79. Kakarougkas,A. and Jeggo,P.A. (2014) DNA DSB repair pathway choice: an orchestrated handover mechanism. *Br. J. Radiol.*, **87**, 20130685.